ELSEVIER

Physica D 78 (1994) 155–165

PHYSICA D

Numerical computations of coarsening in the one-dimensional Cahn–Hilliard model of phase separation ★

Fengshan Bai [a,b,c], Alastair Spence [a], Andrew M. Stuart [d]

[a] *School of Mathematical Sciences, University of Bath, Bath, BA2 7AY, UK*

[b] *Program in Scientific Computing and Computational Mathematics, Stanford University, Stanford, CA 94305, USA*

[c] *Applied Mathematics Department, Tsinghua University, Beijing 100084, China*

[d] *Division of Applied Mechanics, Durand 252, Stanford University, Stanford, CA 94305-4040, USA*

Received 29 September 1993; revised 1 May 1994
Communicated by J.M. Ball

Abstract

Time dependent solutions of the Cahn–Hilliard equation are studied numerically. In particular heteroclinic orbits, which connect different equilibrium solutions at $t = -\infty$ and $t = +\infty$, are sought. Thus boundary value problems in space-time are computed. This computation requires an investigation of the stability of equilibria, since projections onto the stable and unstable manifolds determine the boundary conditions at $t = -\infty$ and $t = +\infty$. This stability analysis is then followed by solution of the appropriate boundary value problem in space-time. The results obtained cannot be found by standard initial value simulations. By specifying the two steady states at $t = \pm\infty$ appropriately it is possible to find orbits reflecting a given degree of coarsening over the time evolution. This gives a clear picture of the dynamic coarsening admissible in the equation. It also provides an understanding of orbits on the global attractor for the equation.

1. Introduction

Consider a binary alloy in a homogeneous mixed state with both components initially uniformly distributed in space. Below a certain critical temperature this configuration is unstable. When such a binary alloy is quenched to a sufficiently low and uniform temperature beneath its critical value, the two components of the alloy tend to separate. The Cahn–Hilliard equation is a phenomenological continuum model for this process, which can be obtained by application of a Helmholtz free energy theory [5]. The equation is posed on $\Omega \subset \mathbb{R}^m$ and is

$$\frac{\partial u}{\partial t} = \Delta w, \quad x \in \Omega,\ t > 0 \tag{1.1}$$

$$0 = \gamma \Delta u + f(u) + w, \quad x \in \Omega,\ t > 0, \tag{1.2}$$

subject to the boundary and initial conditions

$$\nabla u \cdot \boldsymbol{n} = 0, \quad \nabla w \cdot \boldsymbol{n} = 0, \quad x \in \partial\Omega, \quad t > 0, \tag{1.3}$$

$$u(x,0) = u_0(x), \quad x \in \Omega, \tag{1.4}$$

where $\boldsymbol{n}$ denotes the unit outward normal on $\partial\Omega$. Here $u(x,t)$ is an order parameter determining the relative proportions of the two solid phases at point x in space, t in time. The function $w(x,t)$ is the chemical poten-

★ The work of Bai and Spence is supported by the UK Science Engineering Research Council. The work of Stuart is funded by the Office of Naval Research under contract N00014-92-J-1876 and the National Science Foundation under contract number DMS-9201727.

0167-2789/94/$07.00 © 1994 Elsevier Science B.V. All rights reserved
SSDI 0167-2789(94)00133-B

tial which drives the phase separation phenomenon. Integrating (1.1) over Ω and applying (1.3), (1.4) gives

$$\int_{\Omega} u(x,t)dx = \int_{\Omega} u_0(x)dx = M, \quad \forall t \geq 0, \tag{1.5}$$

which implies conservation of total mass.

In this note we consider the simple case of equation (1.1),(1.2) in one space dimension together with

$$f(u) = u - u^3. \tag{1.6}$$

When $u = +1$ the mixture is entirely comprised of one phase and when $u = -1$ it is entirely comprised of the other; $u = 0$ denotes an equal mixture. Our objective is to study numerically the coarsening process. To do this we shall compute time-dependent solutions of (1.1)–(1.3) which connect equilibrium states with differing coarseness properties, to one another. These are known as *connecting* or *heteroclinic orbits*. We note that Eilbeck, Furter and Grinfeld [10] have already computed the equilibrium solutions for this problem and our intended contribution is to determine the dynamics of the equation by studying connecting orbits between these equilibria. Such connections satisfy equations (1.1)–(1.3) subject to

$$\begin{aligned} u(x,t) &\to \omega(x) \quad \text{as } t \to +\infty, \\ u(x,t) &\to \alpha(x) \quad \text{as } t \to -\infty, \end{aligned} \tag{1.7}$$

where $\omega(x)$ and $\alpha(x)$ are two equilibrium solutions satisfying (1.1)–(1.3) with $\partial u/\partial t \equiv 0$. For such a connection to exist it is typically the case that $\alpha(x)$ has a larger number of unstable modes associated with it than does $\omega(x)$. However, since both $\alpha(x)$ and $\omega(x)$ may be unstable we solve (1.1)–(1.3) and (1.7) as a boundary value problem in space and time. It is known that typically [3] the number of unstable spatial modes of an equilibrium grows with the spatial complexity of the solution, reflecting the penalisation of interfacial energy. Hence, for connecting orbits to exist, $\omega(x)$ will be coarser than $\alpha(x)$ and solutions of (1.1)–(1.3) subject to (1.7) thus reflect the coarsening process. From geometric arguments one expects that, to describe a given set of connections between $\alpha(x)$ and $\omega(x)$, one requires p parameters where

$$p = \dim\{W(\alpha(x))\} - \dim\{W(\omega(x))\} - 1, \tag{1.8}$$

and $W(\bar{u})$ denotes the unstable manifold of an equilibrium $\bar{u}$ and $\dim\{\bullet\}$ dimension. (Note that any heteroclinic orbit yields a one parameter family of heteroclinic orbits through time translation; this trivial phase shift parameter is not included in the formula (1.8) for p.)

Such connecting orbits are also of interest in an abstract mathematical context, for the following reason. This system admits a Liapunov function [5,11]: letting $|\bullet|$ denote the standard $L^2(\Omega)$ norm we obtain

$$\begin{aligned} E(u) &= \int_{\Omega} \{\frac{\gamma}{2} |\nabla u|^2 - F(u)\}dx, \\ \frac{d}{dt}\{E(u(t))\} &= -|\nabla w|^2, \end{aligned} \tag{1.9}$$

where $F'(u) = f(u)$; this shows that the Cahn–Hilliard model is a gradient system and that the energy $E(u(t))$ always decreases in time, forcing the solutions to equilibria. Hence by [12], its global attractor is the union of all the equilibrium solutions of (1.1)–(1.3) together with the connecting orbits, satisfying (1.1)–(1.3) and (1.7). For certain reaction diffusion equations the structure of the global attractor has been completely determined analytically [13–15]. It is of interest to extend this work to other equations, and our computational results shed light on this question. Finally, we note that the work of Carr and Pego [7] and Pego [17] indicates that, in one dimension, the phenomenon of metastability is closely related to the properties of solutions on these heteroclinic orbits and this provides a mathematical justification for the physical importance of heteroclinic orbits.

In Section 2 we will briefly describe the spatial approximation we use and describe the basic properties of the spatially discrete equations. In Section 3 we show numerical results for the steady state solutions and their stability properties. Section 4 contains an outline of the computational methods and results for the connecting orbits; this leads us to a conjecture about the structure of the global attractor. Finally, in Section 5 we make some concluding remarks.

2. Numerical methods

We approximate (1.1)–(1.3) in dimension $m = 1$ with $\Omega = (0,1)$ by means of a Galerkin spectral method, using the eigenfunctions $\{\cos(j\pi x)\}_{j=0}^{\infty}$ as a basis. Let $V^N \subset H^1((0,1))$ denote the space $\text{span}\{[\cos(j\pi x)]_{j=0}^{N}\}$ and seek u_N, $w_N \in V^N$ satisfying

$$u_N(x,t) = a_0(t) + \sum_{j=1}^{N} a_j(t)\cos(j\pi x) \tag{2.1}$$

and

$$w_N(x,t) = b_0(t) + \sum_{j=1}^{N} b_j(t)\cos(j\pi x). \tag{2.2}$$

Let $\langle\cdots,\cdots\rangle$ denote the usual L^2 inner product on $(0,1)$. The standard weak form of (1.1)–(1.2) gives us

$$\left\langle \frac{\partial u}{\partial t}, \xi \right\rangle = -\langle \nabla w, \nabla \xi\rangle, \quad \forall \xi \in H^1((0,1)),$$
$$-\gamma\langle \nabla u, \nabla \xi\rangle + \langle f(u) + w, \xi\rangle = 0, \quad \forall \xi \in H^1((0,1)). \tag{2.3}$$

Applying the Galerkin projection and asking that (2.3) hold only for all $\xi \in V^N$, we thus obtain

$$\left\langle \frac{\partial u_N}{\partial t}, \xi \right\rangle = -\langle \nabla w_N, \nabla \xi\rangle, \quad \forall \xi \in V^N,$$
$$-\gamma\langle \nabla u_N, \nabla \xi\rangle + \langle f(u_N) + w_N, \xi\rangle = 0, \quad \forall \xi \in V^N. \tag{2.4}$$

After integrating by parts using (1.3), this yields

$$\left\langle \frac{\partial u_N}{\partial t}, \cos(k\pi x) \right\rangle = (k\pi)^2 \times \left\langle [\gamma \frac{\partial^2 u_N}{\partial x^2} + f(u_N)], \cos(k\pi x) \right\rangle, \quad k = 1,2,\ldots,N.$$

Note that, setting $\xi = 1$ in (2.4), yields

$$\frac{da_0(t)}{dt} = 0,$$

so that we obtain

$$a_0(t) = \int_0^1 u_N(x,t)\,dx = \int_0^1 u_N(x,0)\,dx = M, \quad \forall t \geq 0. \tag{2.5}$$

This is the discrete analogue of the conservation relation (1.5). Using (2.5) we obtain the the following system of ordinary differential equations for $\{a_k(t)\}_{k=1}^{N}$:

$$\frac{da_k(t)}{dt} = (k\pi)^2\left(-\gamma a_k(t) k^2\pi^2 + 2\int_0^1 f(u_N(x,t))\cos(k\pi x)\,dx \right), \tag{2.6}$$

$$a_k(0) = a_k^0 = \int_0^1 u_0(x)\cos(k\pi x)\,dx, \quad k = 1,2,\ldots,N. \tag{2.7}$$

By setting $\xi = \partial u_N/\partial t$ in (2.4) it may be verified that the semi-discrete equations possess the same Liapunov function (1.9) as the original equations and that

$$\frac{d}{dt}\{E(u_N(t))\} = -|\nabla w_N|^2.$$

Hence the approximation is also in gradient form and has a global attractor of the same qualitative type as the underlying partial differential equation.

If we let $A = (a_1, a_2, \cdots, a_N)$ then Eq. (2.6) may be written as

$$\frac{dA}{dt} = G(A). \tag{2.8}$$

Since (2.8) is in gradient form, the global attractor is made up entirely of equilibria and heteroclinic orbits connecting them to one another. Thus to study the global attractor for the approximate system we need only to study the steady states of (2.8) and the connecting orbits between them, satisfying (2.8) and

$$A(t) \to A^+ \quad \text{as } t \to +\infty,$$
$$A(t) \to A^- \quad \text{as } t \to -\infty, \tag{2.9}$$

for $A^{\pm}$ equilibria of (2.8). To compute such connections we apply the approach described in [1] which in

turn relies on the work of Beyn [4]. All the continuation computations in this note are performed by using the package AUTO [9]. The basic idea of the computational technique in [4] is to solve (2.8), (2.9) on a truncated time domain $[-T,T]$; boundary conditions are imposed at $t = T$ (resp. $t = -T$) which project the solution onto the linearised stable (resp. unstable) manifold of A^+ (resp. A^-) at $t = T$ (resp. $t = -T$.) In the case where p given by (1.8) is positive extra conditions are required to parameterise the orbit; once fixed these parameters specify a boundary value problem for (2.8) with the correct number of boundary conditions. An example of such a parameter is (4.1) below.

3. The steady states and their stability

An equilibrium v of the Cahn–Hilliard equation (1.1)–(1.3) in dimension $m = 1$ with $\Omega = (0,1)$ satisfies the following problem: find $v(x)$ such that

$$0 = \gamma \frac{\partial^2 v}{\partial x^2} + f(v) - \int_0^1 f(v)\,dx, \quad x \in (0,1), \quad t > 0, \tag{3.1}$$

$$\frac{\partial v}{\partial x}(0) = \frac{\partial v}{\partial x}(1) = 0, \quad \int_0^1 v(x)\,dx = M, \tag{3.2}$$

where w is a constant by (1.1),(1.3) and (1.2), (1.3) gives its value $w = -\int_0^1 f(v)\,dx$; the mass constraint (1.5) must be specified to obtain isolated solutions. Thus the solution set is parameterized by M and γ. Recall that f is specified by (1.6).

The local bifurcations from the constant trivial solution $u \equiv M$ are studied in [10]. These bifurcations B_k occur at

$$\gamma = b_k = f'(M)/k^2\pi^2, \tag{3.3}$$

and bifurcate in the direction

$$\phi_k = \cos(k\pi x). \tag{3.4}$$

In the case $M = 0$ the trivial solution is $u \equiv 0$ and (3.1),(3.2) satisfy the symmetry

$$u \to (-u). \tag{3.5}$$

The bifurcations are of pitchfork type associated with the breaking of the symmetry (3.5). In the case $M > 0$ the trivial solution is $u \equiv M$ and the symmetry (3.5) no longer holds, but the equations (3.1)–(3.2) are invariant with respect to

$$u(x) \to u(1-x). \tag{3.6}$$

If k is odd this symmetry is broken (as can be seen from (3.4)) and the bifurcations are again of symmetry breaking pitchfork type; however if k is even the bifurcating branches retain the symmetry (3.6). However by carrying out the Liapunov–Schmidt reduction it is found that the bifurcations are still of pitchfork type (see [10]).

We now consider the consequences for stability. Let

$$u = v + e^{\rho t}\phi, \quad w = -\int_0^1 f(v(x))\,dx + e^{\rho t}\theta,$$

where $v(x)$ solves (3.1),(3.2). Substituting in (1.1)–(1.5) and linearising, we obtain the following eigenvalue problem governing the stability of steady solutions of (3.1),(3.2) under (1.1)–(1.5):

$$\rho\phi = \frac{\partial^2 \theta}{\partial x^2}, \tag{3.7}$$

$$0 = \gamma \frac{\partial^2 \phi}{\partial x^2} + f'(v)\phi + \theta, \qquad x \in (0,1), \quad t > 0, \tag{3.8}$$

$$\frac{\partial \phi}{\partial x}(0,t) = \frac{\partial \phi}{\partial x}(1,t) = \frac{\partial \theta}{\partial x}(0,t) = \frac{\partial \theta}{\partial x}(1,t) = 0, \quad t > 0, \tag{3.9}$$

$$\int_0^1 \phi(x)\,dx = 0. \tag{3.10}$$

Note that these equations are invariant under (3.5) for $M = 0$ and (3.6) for $M > 0$, and hence conjugate pairs of solutions breaking the symmetries will have the same stability properties. To be precise, for $M > 0$ with k odd, eigenvalues of (3.7)–(3.10) on conjugate solutions $(v(x),\gamma)$ and $(v(1-x),\gamma)$ are identical, and hence these solutions have identical stability properties. A similar situation arises for $M = 0$ for

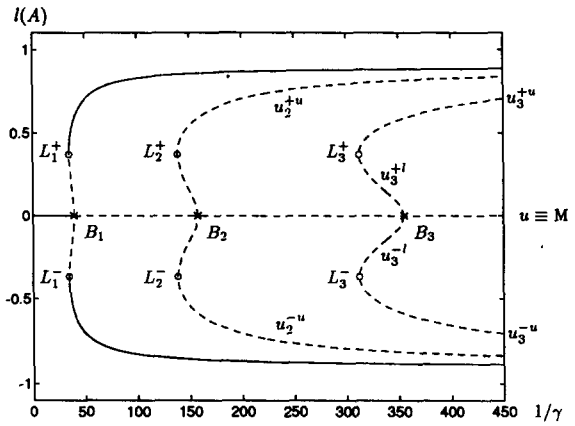

Fig. 1. Notation for equilibria, $l(A) = a_k$, where $|a_k| = \max\{|a_j| : 1 \le j \le N\}$.

all k. However for $M > 0$ with k even the symmetry (3.6) is not broken. Hence no information can be obtained using symmetry arguments about the eigenvalues of (3.7)–(3.10) for points on the upper and lower branches of the pitchfork at the same γ value. Indeed our numerical results show that though the number of positive eigenvalues on these pairs of branches is the same, their values are different depending on which branch is chosen. Thus the quantitative behaviour near each branch differs.

We now describe numerical results. Fig. 1 shows the notation we will use to distinguish different equilibria and different ranges of γ.

Note that the local bifurcation points are labeled B_k with $\gamma = b_k$ given by (3.3). These local bifurcations exist for the physically meaningful case of $\gamma > 0$ only if $0 \le M < 1/\sqrt{3}$; this follows from (1.6),(3.3). A normal form analysis given in [10] shows that the bifurcations are subcritical in γ^{-1}, and hence that turning points $L_k^{\pm}$ exist, only if $M > 1/\sqrt{5}$; the turning points occur at values of γ denoted by $\gamma = l_k$ and satisfy

$$b_1 < l_1 < \infty, \quad b_k < l_k < b_{k-1}, \quad k > 1,$$

provided $1/\sqrt{5} < M < 1/\sqrt{3}$.

Because of the multitude of solutions, the notation in the figures is quite complicated. Here we summarise all the relevant notation. The equilibria are labeled

$$u_k^{+u}, u_k^{-u}, u_k^{+l}, u_k^{-l}. \tag{3.11}$$

Here k is determined by B_k, the local bifurcation point of the branch in question. The index, "u" or "l" distinguishes solutions above ("upper") or below ("lower") the solution at the turning point $L_k^{\pm}$ in norm, see Fig. 1. The index $\pm$ distinguishes solutions which bifurcate from $u \equiv M$ along the directions $\pm\phi_k$, given by (3.4), at $\gamma = b_k$. The following modifications of the notation (3.11) will also be used to cover the variations on the situation just outlined:

(i) note that all solutions in (3.11) depend upon γ and, where this dependence is important, we shall denote it by use of the notation $u_k^{+u}(\gamma)$ etc.;

(ii) note that the indices l, u in notation (3.11) are redundant if $0 \le M < 1/\sqrt{5}$ where no turning points are observed. In this case they will be dropped;

(iii) the notation (3.11) will be extended to the case $1/\sqrt{3} < M < 1$, where no local bifurcations occur, by appealing to continuity in M in a straightforward way.

Solutions for (3.1),(3.2) are given in Fig. 2, where solid lines represent stable branches and dashed lines represent unstable branches. Note that numbers on the solution branches in Figs. 2a,c,e give the value of $\dim\{W(\bar{u})\}$ – the dimensions of the unstable manifolds of $\bar{u}$; "o" are turning points and "x" are bifurcation points in both Figs. 1 and 2. The computations agree with known analytical results concerning stability, see [6] and [2].

3.1. *The parameter regime* $0 \le M < 1/\sqrt{5}$

Figs. 2a and b show the steady state solutions computed for $M = 0$, where (a) shows the L^2 norm of u versus the parameter γ^{-1} and (b) plots the largest component (in absolute value) of the Fourier modes. The bifurcations are supercritical in this case, as shown by the local bifurcation analysis in [10]. The kth bifurcation point we denote by B_k with $\gamma = b_k$. Thus, by points (i) and (ii) above, we denote by $u_k^{\pm}(\gamma)$ the two branches bifurcating from B_k. For the case of $M = 0$, it is proved in Bates and Fife [3] that

$$\dim\{W(u_k^{\pm}(\gamma))\} = k - 1, \quad k = 1, 2, \ldots. \tag{3.12}$$

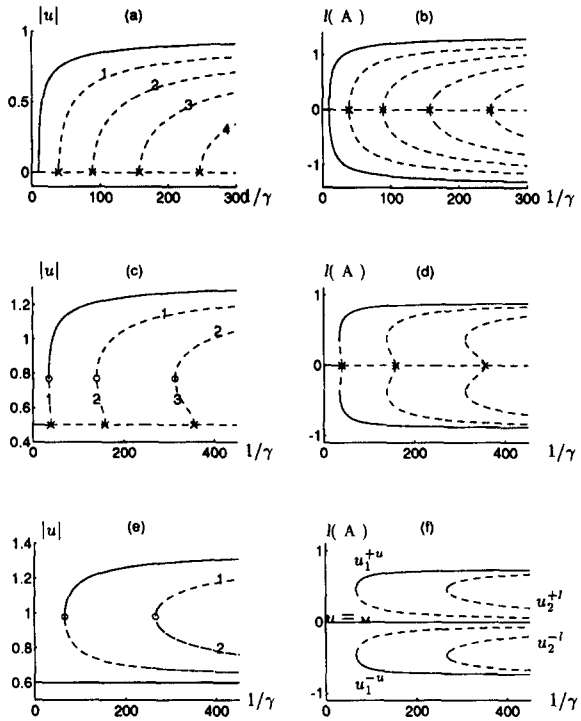

Fig. 2. Steady state solution, $l(A) = a_k$, where $|a_k| = \max\{|a_j| : 1 \le j \le N\}$.

For the general case of $0 < M < 1/\sqrt{5}$, no theoretical results are known about the dimension of the unstable manifold, but we believe that (3.12) still holds since the bifurcation remains subcritical and no turning points are observed on the nontrivial solutions. Numerical results confirm this conjecture.

3.2. *The parameter regime* $1/\sqrt{5} < M < 1/\sqrt{3}$

The local bifurcations are now subcritical. Figs. 2c and d show the steady state solutions computed for $M = 0.5$; recall that the kth bifurcation point is B_k, where $\gamma = b_k$, and that there are turning points $L_k^{\pm}$, located at $\gamma = l_k$. Recalling the notation from (3.11) we have that

$$|u_k^{\pm u}(\gamma)| > |u_k^{\pm}(l_k)|,$$
$$|u_k^{\pm l}(\gamma)| < |u_k^{\pm}(l_k)|, \quad \forall \gamma < l_k,$$

where

$$u_k^{\pm}(l_k) \equiv u_k^{\pm u}(l_k) \equiv u_k^{\pm l}(l_k).$$

The dimension of the unstable manifold of $u_k^{\pm}(\gamma)$ changes at the turning point. Numerically, we observe that for $k = 1, 2, \ldots,$

$$\dim\{W(u_k^{\pm u}(\gamma))\} = k - 1,$$
$$\dim\{W(u_k^{\pm l}(\gamma))\} = k, \quad \gamma < l_k. \tag{3.13}$$

3.3. *The parameter regime* $1/\sqrt{3} < M < 1$

No local bifurcations exist in this range. Figs. 2e and f show the steady state solutions computed for $M = 0.6$. As mentioned in (iii) above we denote by $u_k^{\pm}(\gamma)$ the kth pair of nontrivial branches counting from the left. A continuity argument in M shows that this notation is analogous to that used in the previous parameter range for M. Numerically we observe that the dimension of the unstable manifold is as described by (3.13).

4. Results for heteroclinic orbits

Throughout the following we use the notation detailed in the last section for the steady solutions of the problem and for bifurcation and turning points. (Notice that the steady state bifurcation diagrams in the last section are plotted against $1/\gamma$ rather than the parameter γ itself.) In the heading of the examples, $\alpha(x)$ and $\omega(x)$ denote the α and ω limit sets of the computed heteroclinic orbit respectively, where the α limit set is the equilibria at $t = -\infty$ and the ω limit set the equilibria at $t = +\infty$.

Our objective here is simply to determine the answers to the following two questions: (i) *which equilibria are connected via heteroclinic orbit(s)?*; (ii) *how many parameters are required to describe the heteroclinic orbits between any given α and ω limit sets?* The answers to these questions are completely resolved for a certain reaction-diffusion equation (the Chafee–Infante problem) [8,12,13] and some of what we say will involve relating the Cahn–Hilliard equation to that Chafee–Infante equation by use of the theory of Mischaikow [15].

Finding a connection involves solving a nonlinear boundary value problem and the primary difficulty

here is to determine an initial starting guess for the computations. This issue is resolved by using the techniques described in [1].

4.1. The parameter regime $0 \leq M < 1/\sqrt{5}$

For $M = 0$, Mischaikow [15] has proved that on a subset of the global attractor the dynamics of (1.1)–(1.5) are semi-conjugate to the dynamics of the Chafee–Infante problem [12,13], for any $\gamma \neq b_k$. Thus in this case, a certain subset of the connecting orbit set is completely understood. Our numerical computations do not reveal any connecting orbits other than those predicted in [15].

Furthermore, if our conjecture that (3.12) is true for all $M \in [0, 1/\sqrt{5})$, then the theory of [15] applies and again the dynamics on a subset of the global attractor are equivalent to the dynamics of the Chafee–Infante equation. Our numerical experiments indicate that, as for $M = 0$, the *only* connecting orbits for $0 \leq M < 1/\sqrt{5}$ are precisely those predicted by [15].

4.2. The parameter regime $1/\sqrt{5} < M < 1/\sqrt{3}$ and $l_{k+1} < \gamma < b_k$ for $k = 1, 2, \ldots$

For this range of M turning points may be found in the bifurcation diagram and the theory of [15] does not apply. Nonetheless if $l_{k+1} < \gamma < b_k$, the number of solutions is identical to the number for $b_{k+1} < \gamma < b_k$ if $0 \leq M < 1/\sqrt{5}$ since the extra equilibrium solutions introduced by those turning points do not exist in $\gamma \in (l_{k+1}, b_k)$ (cf. Figs. 1 or 2c and 2d). Furthermore the stability properties are also identical. Our computations indicate that, again, the structure of the connecting orbit set is identical to that found for $M = 0$, $b_{k+1} < \gamma < b_k$.

4.3. The parameter regime $1/\sqrt{5} < M < 1/\sqrt{3}$ and $b_k < \gamma < l_k$ for $k = 1, 2, \ldots$

In this regime a fundamentally new structure arises in the global attractor, due to the presence of extra equilibria introduced at turning points. We describe this by means of examples.

Example 4.1. $\alpha = u_3^{+l}(\gamma)$, $\omega = u_2^{-u}(\gamma)$, $\gamma^{-1} = 344$, $M = 0.5$. We consider first connections between $u_3^{+l}(\gamma)$ and $u_2^{-u}(\gamma)$, for $b_3 < \gamma < l_3$. See Fig. 1 or Fig. 2b. It then follows from (3.13) that $u_3^{+l}(\gamma)$ has an unstable manifold of dimension 3 and $u_2^{-u}(\gamma)$ has as unstable manifold of dimension 1. Since one free parameter is needed to eliminate the non-uniqueness in time due to the phase shift we deduce from (1.8) that such connections are parameterized by a single real number, for which we take

$$\mu = \int_0^1 a_3^2(\tau)\, d\tau. \tag{4.1}$$

Here τ is a rescaling of time to place the computed connection on a unit interval in time, see [1] for details.

Figs. 3a–d show a sequence of connecting orbits for values of $\mu \in (0, 0.0155)$. In Fig. 3d, where μ is at its biggest, the connecting orbit passes close to the solution $u_3^{+u}(\gamma)$ before finally reaching $u_2^{-u}(\gamma)$ at $t = +\infty$. Similarly, Fig. 3a, where μ is at its smallest, the connecting orbit passes close to the constant solution M, before finally reaching $u_2^{-u}(\gamma)$ at $t = +\infty$. Thus Fig. 3 contains a sequence of connections occupying the left-hand lower quadrant of Fig. 7.

The other kinds of connections for $b_3 < \gamma < l_3$ are more straightforward and are given by the following three examples.

Example 4.2. $\alpha = u_3^{+l}(\gamma)$, $\omega = u_3^{+u}(\gamma)$, $\gamma^{-1} = 344$, $M = 0.5$. From (1.8), (3.13) a single connection exists n this case; the result is shown in Fig. 4.

Example 4.3. $\alpha = u_3^{+l}(\gamma)$, $\omega = M$, $\gamma^{-1} = 344$, $M = 0.5$. From (1.8), (3.13) a single connection exists in this case; the result is shown in Fig. 5.

Example 4.4. $\alpha = M$, $\omega = u_2^{-u}(\gamma)$, $\gamma^{-1} = 344$, $M = 0.5$. From (1.8), (3.13) a single connection exists in this case; the result is shown by the Fig. 6.

Remark 4.1. Fig. 7 shows the structure of heteroclinic orbits obtained by our numerical computations for $b_3 < \gamma < l_3$. We have not proved this structure but

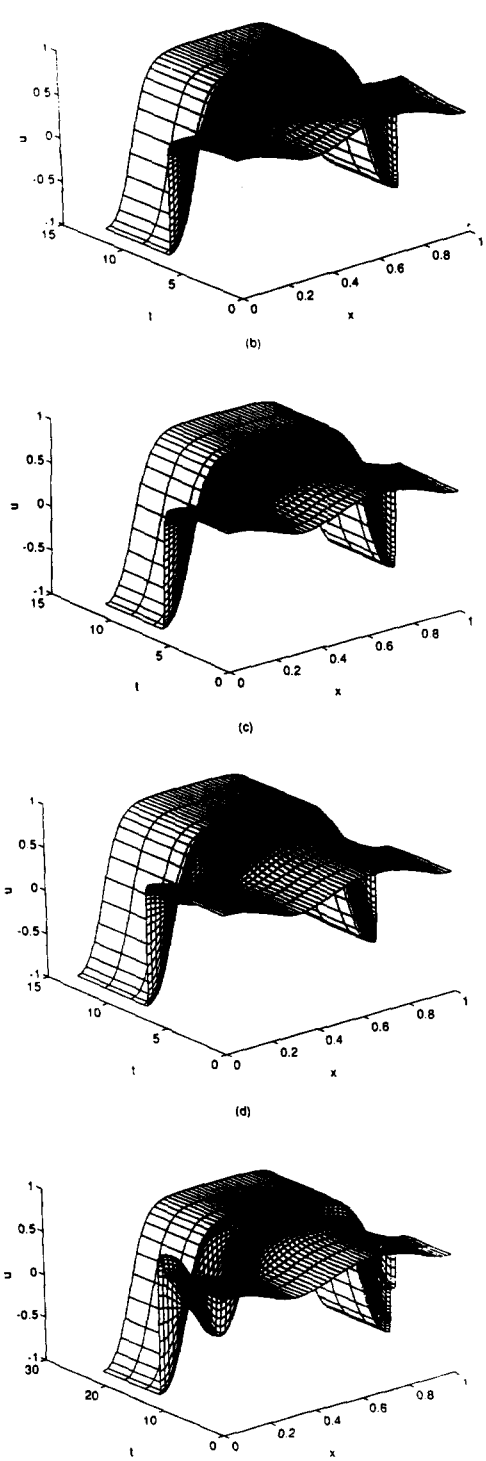

Fig. 3. Connections for $\alpha = u_3^{+l}(\gamma)$, $\omega = u_2^{-u}(\gamma)$, $\gamma^{-1} = 344$, $M = 0.5$. (a) $\mu = 4.20 \times 10^{-3}$; (b) $\mu = 6.03 \times 10^{-3}$; (c) $\mu = 8.04 \times 10^{-3}$; (d) $\mu = 1.55 \times 10^{-2}$.

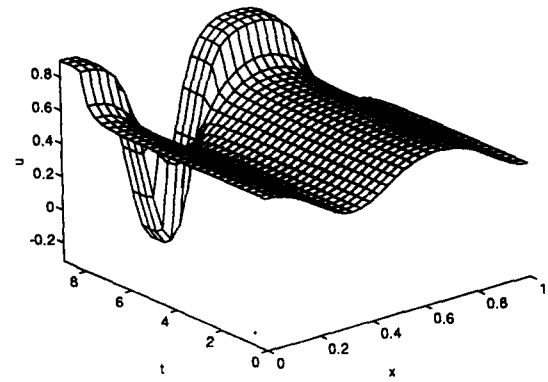

Fig. 4. The connection for $\alpha = u_3^{+l}(\gamma)$, $\omega = u_3^{+u}(\gamma)$, $\gamma^{-1} = 344$, $M = 0.5$.

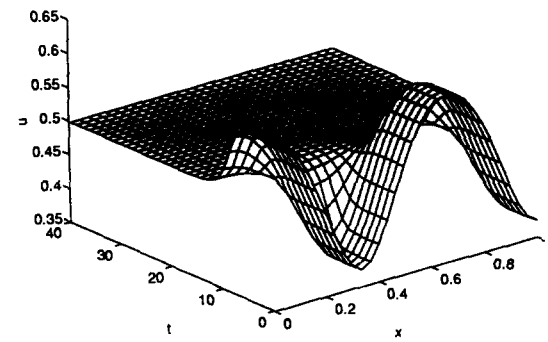

Fig. 5. The connection for $\alpha = u_3^{+l}(\gamma)$, $\omega = M$, $\gamma^{-1} = 344$, $M = 0.5$.

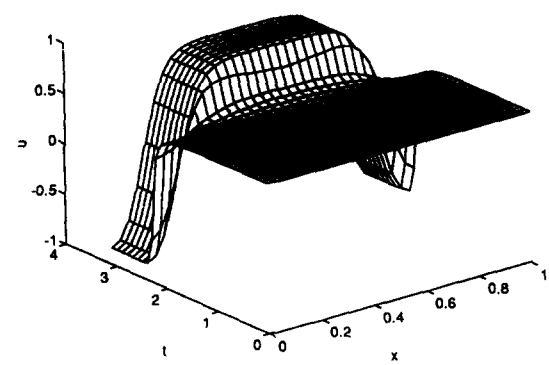

Fig. 6. The connection for $\alpha = M$, $\omega = u_2^{-u}(\gamma)$, $\gamma^{-1} = 344$, $M = 0.5$.

the computations described and further experimentation we are about to describe strongly support it. From the analysis of Mischaikow [16,15] it follows that there are four possibilities for the phase portrait at $M = 0.5$, $b_3 < \gamma < l_3$, including that depicted in

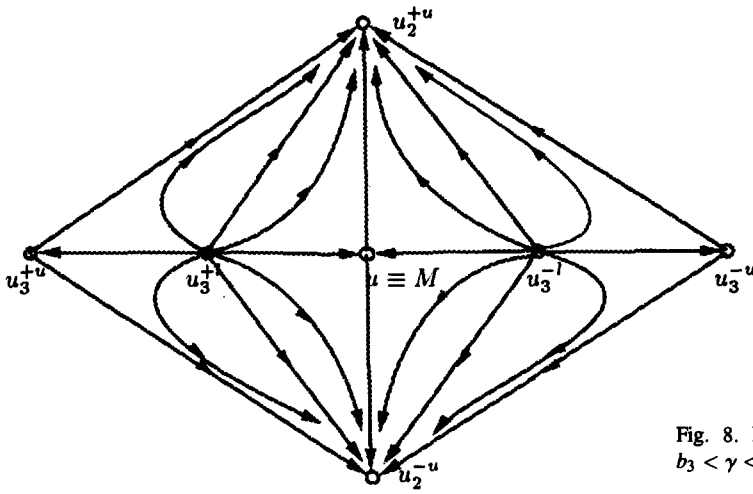

Fig. 7. Structure of heteroclinic orbits at $M = 0.5$, $b_3 < \gamma < l_3$.

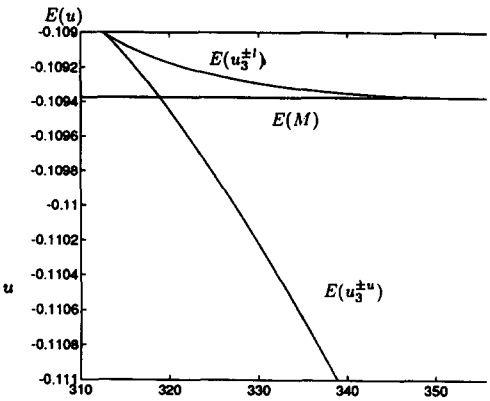

Fig. 8. Numerical relative energy levels with $M = 0.5$, a $b_3 < \gamma < l_3$.

Fig. 7. We have been unable to eliminate the other three possibilities but computations make them appear very unlikely. The other three possibilities occur only if global bifurcations yield heteroclinic connections between equilibria with $\alpha(x)$ and $\omega(x)$ satisfying

$$\dim\{W(\alpha)\} = \dim\{W(\omega)\}, \tag{4.2}$$

(violating (1.8)). In order for this happen we require $E(\omega) < E(\alpha)$ by (1.9). Thus in order to try and computationally eliminate such global bifurcations between equilibria satisfying (4.2), it is necessary to understand the behaviour of $E(\bar{u}(\gamma))$. Fig. 8 shows the behaviour of $E(\bar{u}(\gamma))$ for $\bar{u}(\gamma) = u_3^{\pm}(\gamma)$ and $\bar{u}(\gamma) \equiv M$. Note that

$$\dim\{W(u_3^{\pm u})\} = \dim\{W(M)\} = 2.$$

Using Fig. 8 we obtain some knowledge of parameter regimes where global heteroclinic bifurcations may occur and then try to eliminate such a possibility by means of computation. This does not constitute a proof but we find no evidence of the necessary global bifurcations and hence conjecture that Fig. 7 is correct.

4.4. *The parameter regime* $1/\sqrt{3} < M < 1$

In this regime the structure of the global attractor becomes much more complicated, due to the presence of extra equilibria introduced at turning points as γ · 0. In particular, if $\gamma < l_1$ there is now one more stat solution if $M > 1/\sqrt{3}$ than there is for $M < 1/\sqrt{}$ since the trivial solution $u \equiv M$ is stable for all We illustrate the effect of this on the connecting orl structure by means of examples.

Example 4.5. $\alpha = u_2^{-l}(\gamma)$, $\gamma^{-1} = 333, M = 0.6$.. See Fig. 2f. The linear unstable manifold at u_2^{-l} is tv dimensional and generated by $span\{\eta_1, \eta_2\}$, whe η_1 and η_2 are eigenvectors satisfying (3.7)–(3.1 with $v = u_2^{-l}$. We then take initial conditions as

$$u_0 = u_2^{-l}(\gamma) + \epsilon_1\eta_1 + \epsilon_2\eta_2,$$

where ϵ_j are small. In Fig. 9, (a) is for $\epsilon_1 = 10^{-8}, \epsilon_2$ 10^{-6}; (b) is for $\epsilon_1 = 10^{-7}, \epsilon_2 = 10^{-6}$; (c) is for ϵ_1 $-10^{-7}, \epsilon_2 = 10^{-6}$.

If $M < 1/\sqrt{3}$ then almost all initial data starti near $u_2^{-l}(\gamma)$, $\gamma < l_2$ converge to $u_1^{\pm}(\gamma)$ as $t \to$ c However, as our computation results in Fig. 9 ha shown, if $M > 1/\sqrt{3}$ then there are *three* stable a tracting solutions for initial data starting near $u_2^{-l}(\gamma$ This means that continuation of heteroclinic conne tions in M for $M < 1/\sqrt{3}$ to $M > 1/\sqrt{3}$ may e counter difficulties and indeed we have observed th

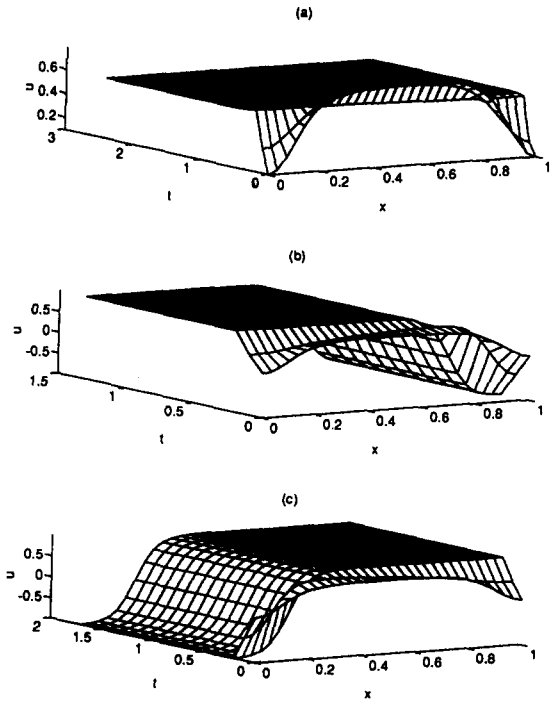

Fig. 9. Connections for $M = 0.6$.

5. Conclusions and remarks

In this paper we have described the application of a computational technique, specifically designed to capture the dynamical behaviour of gradient partial differential equations, to the Cahn–Hilliard model of phase transitions. We have interpreted the coarsening process as a connecting orbit in phase space and investigated the parameter dependence of such orbits as the mass constraint is varied. This has led to a conjecture about the structure of the global attractor, see Fig. 7. Whilst there is probably nothing contentious about the conjecture and broad agreement could probably be obtained that it is *likely* to be correct, we believe that such computations are valuable in this context. This is since: (a) the computations lend further weight to the conjecture and (b) the computations give quantitative structure of orbits on the attractor. It is hoped that further knowledge about the structure of attractors for other partial differential equations can be obtained by using the computational technique described here to compute heteroclinic and homoclinic orbits.

Acknowledgements

We are very grateful to Konstantin Mischaikow and Gerald Moore for helpful suggestions and discussions.

References

[1] F. Bai, A. Spence and A.M. Stuart, The numerical computation of heteroclinic connections in systems of gradient partial differential equations, SIAM J. Appl. Math. 53 (1993) 743–769.

[2] P. Bates and P. Fife, The dynamics of nucleation for the Cahn–Hilliard equations, SIAM J. Appl. Math. 53 (1993) 990–1008.

[3] P. Bates and P. Fife, Spectral comparison principles for the Cahn–Hilliard and phase field equations, and time scales for coarsening, Physica D 43 (1990) 335–348.

[4] W.J. Beyn, The numerical computation of connecting orbits in dynamical systems, IMA J. Numer. Anal. 9 (1990) 379–405.

[5] J.W. Cahn and J.E. Hilliard, Free energy of a non-uniform system I. Interfacial free energy, J. Chem. Phys. 28 (1958) 258–267.

[6] J. Carr, M.E. Gurtin and M. Slemrod, Structured phase transitions on a finite interval, Arch. Rat. Mech. Anal. 86 (1984) 317–351.

[7] J. Carr and R.L. Pego, Metastable Patterns in Solution of $u_t = \epsilon^2 u_{xx} - f(u)$, Comm. Pure Appl. Math. 42 (1989) 523–576.

[8] N. Chafee and E.F. Infante, A bifurcation problem for a nonlinear partial differential equation of parabolic type, J. Appl. Anal. 4 (1974) 17–35.

[9] E.J. Doedel and J.P. Kernĕvez, AUTO: Software for Continuation and Bifurcation Problems in Ordinary Differential Equations, Appl. Math. Report, Caltech (1986).

[10] J. Eilbeck, J. Furter and M. Grinfeld, On a stationary state characterization of transition from spinodal decomposition to nucleation behaviour in the Cahn–Hilliard model of phase separation , Phys. Lett. A 135 (1989) 272–275.

[11] C.M. Elliott and S. Zheng On the Cahn–Hilliard equation, Arch. Rat. Mech. Anal. 96 (1986) 339–357.

[12] J.K. Hale, Asymptotic behaviour of dissipative systems, Am. Math. Surveys Monographs, vol. 25 (AMS, Providence, 1988).

[13] D. Henry, Geometric Theory of Semilinear Parabolic Equations, Lect. Notes in Math., vol. 840 (Springer, Berlin, 1981).

[14] D. Henry, Some infinite dimensional Morse–Smale systems defined by parabolic differential equations, J. Diff. Eq. 59 (1985) 165–205.

[15] K. Mischaikow, Global asymptotic dynamics of gradient-like bistable equations, CNSNS92-94, Georgia Tech., preprint.

[16] K. Mischaikow (1993), Private communication.

[17] R.L. Pego, Front migration in the nonlinear Cahn–Hilliard equation, Proc. Roy. Soc. London Ser. A 422 (1989) 261–278.

[18] R. Temam, Infinite-Dimensional Dynamical Systems in Mechanics and Physics, Appl. Math. Sci., vol. 68 (Springer, Berlin, 1988).